

Inviscid coalescence of drops

By L. DUCHEMIN¹, J. EGGERS² AND
C. JOSSERAND³

¹Department of Mathematics, Imperial College of Science, Technology and Medicine, 180
Queen's Gate, London, SW7 2BZ, UK

²Fachbereich Physik, Universität Gesamthochschule Essen, 45117 Essen, Germany

³Laboratoire de Modélisation en Mécanique, 8, rue du Capitaine Scott, 75015 Paris, France

(Received 28 September 2018)

We study the coalescence of two drops of an ideal fluid driven by surface tension. The velocity of approach is taken to be zero and the dynamical effect of the outer fluid (usually air) is neglected. Our approximation is expected to be valid on scales larger than $\ell_\nu = \rho\nu^2/\sigma$, which is $10nm$ for water. Using a high-precision boundary integral method, we show that the walls of the thin retracting sheet of air between the drops reconnect in finite time to form a toroidal enclosure. After the initial reconnection, retraction starts again, leading to a rapid sequence of enclosures. Averaging over the discrete events, we find the minimum radius of the liquid bridge connecting the two drops to scale like $r_b \propto t^{1/2}$.

1. Introduction

Drop coalescence arises in many different contexts, and is crucial to our understanding of free surface flows (Eggers 1997). Examples are printing applications (Chaudhary & Maxworthy 1980; Wallace 2001), drop impact on a fluid surface (Oguz & Prosperetti 1990), and the coarsening of drop clouds and dispersions (MacPhee *et al.* 2002; Jury

et al. 1999; Verdier 2000). After the two surfaces have merged on a microscopic scale, surface tension drives an extremely rapid motion, usually impossible to resolve in either experiment (Bradley & Stow 1978; Menchaca-Rocha *et al.* 2001) or simulation (Lafaurie *et al.* 1994). Thus theory is needed to investigate a possible dependence on initial conditions, development of small-scale structures during merging, and to estimate the typical time required for merging.

A large body of work exists on this problem in the case that viscosity is dominant and the motion is described by Stokes' equation. In the absence of an outer phase this is known as the "viscous sintering problem" (Frenkel 1945; Hopper 1993; Martinez-Herrera & Derby 1995), the inclusion of an outer phase is important for many problems governing the coarsening of dispersion (Nikolayev *et al.* 1996; Verdier 2000). For the two-dimensional problem (i.e. for the merging of cylinders) *exact* solutions exist (Hopper 1990; Richardson 1992; Crowdy 2002, To appear), which were shown (Eggers *et al.* 1999) to be asymptotically equivalent to their three-dimensional counterparts. The presence of an outer fluid leads to the formation of a toroidal bubble during merging (Eggers *et al.* 1999), significantly modifying the dynamics.

Fig. 1 shows two equal drops of radius R being connected by a liquid bridge of radius r_b , which is rapidly being pulled up by surface tension. The local Reynolds number of this flow can be estimated as $Re = \sigma r_b / (\rho \nu^2)$, where σ is the surface tension, ρ the density, and ν the kinematic viscosity. Thus, regardless of the value of the viscosity, the Reynolds number is always small in the initial phases of the merging, which is equivalent to demanding that $r_b \ll \ell_\nu$, where $\ell_\nu = \nu^2 \rho / \sigma$ is the viscous length scale. However, ℓ_ν is often very small (140 Å for water, and 4 Å for mercury (Eggers 1997)), so $r_b \gg \ell_\nu$ for a large part of the evolution, and inviscid theory can be applied. Thus for a wide range of practical problems the almost inviscid regime, which is the topic of this letter, is the

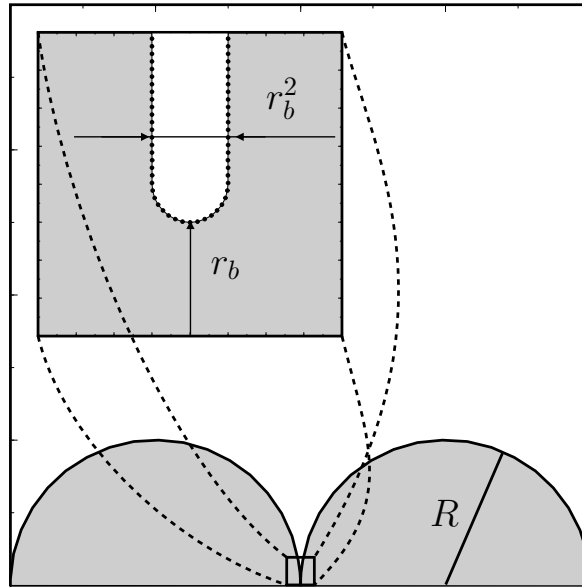


FIGURE 1. Initial condition. Two drops touching at a point are joined by a liquid bridge of radius r_b . The inset shows the width of the gap just above the meniscus to be $w = r_b^2$. The gap's walls are nearly straight on the scale of w .

most relevant. Typically, the viscous regime will serve as an inner layer that defines the initial condition for the inviscid problem we are interested in. In general, we do not have to worry about the initial process of reconnection (Amarouchene *et al.* 2001), which for clean fluids is expected to take place over a microscopically small area.

In the case of a head-on collision of two drops with relative velocity V , considered in (Oguz & Prosperetti 1989), a purely geometrical consideration predicts $r_b \approx \sqrt{VRt}$ for two overlapping circles. The corresponding speed of merging is of the same order as the surface-tension-driven merging to be described below, so V has thus to be taken into account. However, we will restrict ourselves here to the case where the velocity of approach is vanishingly small, a condition that is easily realizable experimentally (Menchaca-Rocha *et al.* 2001). We also do not treat the dynamical effect of an outer fluid like air, which might become important as the lubrication layer between the approaching

drops becomes very thin (Eggers *et al.* 1999; Yiantsos & Davis 1991). However, this approximation is consistent with the assumption of a small velocity of approach.

2. Initial conditions and scaling laws

We consider two identical drops of radius R touching at a point where a thin liquid bridge of size r_b connects the two drops initially (cf. figure 1). The general problem of drops of different radii only changes a prefactor in the gap width between the drops (Eggers 1998). For the inviscid dynamics considered here, all parameters of the problem can be scaled out by writing the time and space coordinates in units of $\sqrt{\rho R^3/\sigma}$ and R , respectively. Assuming that the vorticity generated by the initial viscous motion can be neglected, and using incompressibility, the velocity potential φ obeys

$$\Delta\varphi = 0. \quad (2.1)$$

The boundary condition on the free surface amounts to a balance between surface tension and Bernoulli pressures (Oguz & Prosperetti 1989):

$$\frac{\partial\varphi}{\partial t} + \frac{1}{2}(\nabla\varphi)^2 - \kappa = 0, \quad (2.2)$$

where κ is the mean curvature of the interface.

We have to solve (2.1),(2.2) with the initial condition shown in figure 1, assuming that the bridge radius r_b is initially very small (typically 10^{-5} in our numerical simulations). Away from the point of contact at $z = 0$, but for $h \ll 1$ the surface has the form $h(z) = (2z)^{1/2}$ and $h(z) = (-2z)^{1/2}$ for $z > 0$ and $z < 0$, respectively. The width of the gap at a height r is thus

$$w = r^2 \quad (r_b \ll r \ll 1) \quad (2.3)$$

and since $\partial w/\partial r \ll 1$, the walls are nearly parallel. Thus the meniscus, which owing to

radial symmetry is located along a ring of radius r_b , is being pulled straight up by a force 2σ per unit length.

Assuming that the profile in region (2.3) matches onto the bridge on the scale $r \approx r_b$, the curvature at the meniscus can be estimated as $\kappa_b \approx r_b^{-2}$, much larger than the axial curvature r_b^{-1} of the liquid bridge. Thus, as already argued in (Eggers *et al.* 1999), the axial curvature can be neglected for $r_b \ll 1$ and the problem becomes effectively two-dimensional, equivalent to the merging of two fluid cylinders. Thus a model problem (Oguz & Prosperetti 1989; Eggers 1998) for the initial motion of the meniscus is that of the two dimensional, *straight* slot shown in the inset of figure 1. The eventual widening of the gap can be neglected on the scale of the gap width w .

The results of our computations for the full three-dimensional problem, to be explained in more detail below, are shown in figure 2. As the meniscus retracts, the rapid fluid flow past the sides of the gap creates an under-pressure as described by Bernoulli's equation (2.2), which in turn causes the end to expand into a bubble. As the bubble increases in size, capillary waves are excited in its wake, with amplitude roughly proportional to the bubble radius. Thus after the amplitude of the capillary wave has grown to the half width of the slot $w/2$, its two sides touch and reconnect at a time τ_c . Since the width is the only length scale in the problem, it follows that the total length r_c the meniscus has retracted up to the point of reconnection is proportional to w , while the time τ_c required scales like $w^{3/2}$. We thus have

$$r_c = r_0 w, \quad \tau_c = \tau_0 w^{3/2}, \quad (2.4)$$

where r_0, τ_0 are constants to be determined numerically. Below we find in fact $r_0 = 10, \tau_0 = 7.6$.

After the two sides of the gap have reconnected, this new initial condition looks very similar to the original one, except for a non-trivial velocity field that remains. But since

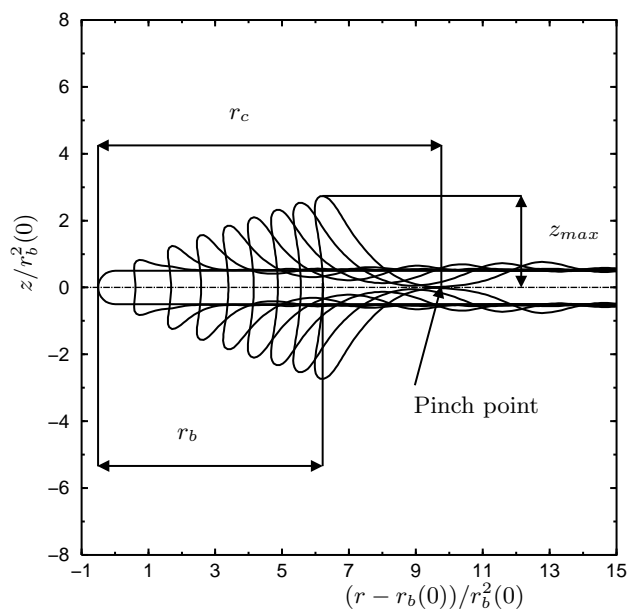


FIGURE 2. A sequence of profiles showing the retraction of the initial meniscus for $r_b(0) = 10^{-5}$. At a time $\tau_c = \tau_0 w^{3/2} = 7.6 w^{3/2}$ the walls of the gap touch and the minimum radius z_{min} goes to zero. The distance of this point from the initial tip of the meniscus is $r_c = r_0 w = 10 w$.

most of the resistance to the motion *before* reconnection is due to the large bubble that was left behind, this velocity can be neglected relative to the velocity to be generated at the next stage of the motion (more detailed estimates are given below). This means that at each step the same motion repeats itself, but with a slightly larger radius r_b . At the n -th step we can thus write, analogous to (Eggers 1998),

$$r_b^{n+1} - r_b^n = r_c = r_0 (r_b^n)^2,$$

and for the times t_n of successive pinching events:

$$t_{n+1} - t_n = \tau_0 (r_b^n)^3.$$

For very small initial r_b reconnection occurs in rapid succession, with small relative change of the variables. We can thus write r_b as a smooth function of t , obeying the

differential equation

$$\frac{dr_b}{dt} \approx \frac{r_0}{\tau_0} \frac{1}{r_b} \quad (2.5)$$

which gives, after integration :

$$r_b \approx \sqrt{\frac{2r_0}{\tau_0} t^{1/2}}. \quad (2.6)$$

The scaling law (2.6) is the central result of the present letter. Eventually, when r_b is of the same order than the drop radius, the widening of the channel overcomes the growth of capillary waves, and the enclosure of bubbles stops. This is when the time scale of retraction $\tau \approx r_b^2 \tau_0 / (2r_0)$ is shorter than $\tau_c \approx \tau_0 r_b^3$ characterizing reconnection. Thus reconnection will cease when $r_b \gtrsim 1/(2r_0) = 0.05$. We have determined numerically that no more voids are entrapped for $r_b > 0.035$, in good agreement with our theoretical estimate. Below we present detailed numerical tests of the scaling predictions, and investigate further the crucial stage of bubble growth, from which we are able to extract the numerical constants r_0, τ_0 .

3. Boundary integral method

If the flow can be considered potential and incompressible, the use of a boundary integral method is advantageous, since the velocity field can be calculated from the interface shape. Thus one only needs to keep track of the interface, represented by a one-dimensional curve, and grid refinement can be done very efficiently. The majority of these boundary integral methods require smoothing of the surface, in order to avoid short wave length instabilities. The method briefly presented here does not require any explicit smoothing, except for a redistribution of the points around the tip at every time step. This redistribution can act as a smoothing, but no damping of instabilities, such as an artificial surface viscosity, has been used.

The dipole formulation used here is very close to the one described by Baker, Meiron

and Orszag (Baker *et al.* 1980), but it needs to be refined to be able to resolve the very disparate scales of the drops and of the highly curved region close to the meniscus. At a given time step, we expect the velocity potential φ to be known, from which we calculate the normal and the tangential velocity of the surface. This velocity is then used to advect the surface, and to advance φ using Bernoulli's equation (2.2). The tangential velocity is calculated directly by differentiating with respect to the arclength along the interface:

$$u_t = \frac{\partial \varphi}{\partial s} \quad (3.1)$$

to compute the normal component, we use the vector potential \mathbf{A} of the velocity field, $\mathbf{u} = \nabla \times \mathbf{A}$:

$$u_n = \frac{1}{r} \frac{\partial r A_\theta}{\partial s}. \quad (3.2)$$

Following (Baker *et al.* 1980), we first compute the dipole density μ from

$$\varphi(M) = \mu(M) + \frac{1}{4\pi} \int_S (\mu(M) - \mu(M')) \frac{\partial}{\partial n} \left(\frac{1}{\lambda} \right) dS', \quad (3.3)$$

where λ is the distance between points M and M' on the surface. The appearance of $\mu(M)$ in the integrand serves to subtract the singularity of the normal derivative. Once μ is known, it can be used to calculate the vector potential:

$$\mathbf{A}(M) = \frac{1}{4\pi} \int_S (\mu(M') - \mu(M)) \mathbf{n} \times \nabla_s \left(\frac{1}{\lambda} \right) dS'. \quad (3.4)$$

Classical iterative solutions of (3.3),(3.4) were found to fail for very small bridge radii, so (3.3),(3.4) were solved by matrix inversion instead. A simple trapezoidal rule was used to convert the equations into linear systems, which was then solved by LU decomposition. In order to compute the curvature of the surface and the tangential derivatives in (3.1),(3.2), we re-parametrized the integrals by introducing a new integration variable ζ , which equals i at grid-point i . This avoids instabilities in the cubic spline interpolation

that would otherwise be present if two points come very close together, as it happens at the tip.

At each time step, the Bernoulli equation and the kinematic condition were used to advance the solution using a Crank-Nicolson scheme (Press *et al.* 1992). The implicit equations were solved by iteration, which required less than 10 iterations until a relative error of 10^{-5} in the velocity potential was reached. An explicit Runge-Kutta fourth order scheme was also tested, but found to be too unstable for small values of r_b .

We also redistribute grid-points at every time step according to their distance from the tip. Cubic splines are used to interpolate to the new points. At each time step points are placed on the free surface with grid spacing δ ; typical values are shown in figure 3. This spacing is used up to a distance of $40r_b^2$ from the tip, after which it is gradually increased in steps of 2, since much lower resolution is required far from the tip.

4. Reconnection

As we have explained above, the retraction of the meniscus is interrupted by the reconnection of the two sides of the gap, and the distance r_c by which the meniscus recoils as well as the time τ_c required is given by the scaling relations (2.4). In figure 2 we define typical quantities characterizing the retraction of the meniscus. The minimum gap radius z_{min} marks the first trough of a train of capillary waves that is generated by the growing bubble. Note that in the corresponding simulation in (Oguz & Prosperetti 1990) (cf. figure 4) there is little or no indication of this growth of capillary waves. We suspect that these authors did not follow the retraction for sufficiently long times, and that the low resolution of their simulation introduced additional damping, which smoothed out the capillary waves.

As seen in figure 3, the time dependence of the minimum gap radius z_{min} converges

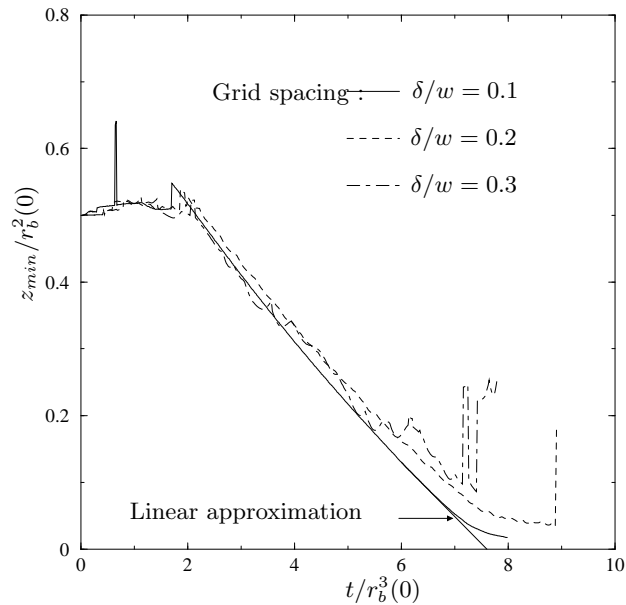


FIGURE 3. The minimum gap radius $z_{min}/r_b^2(0)$ plotted against $t/r_b^3(0)$. The initial value of r_b is 10^{-5} and the three resolutions correspond to the minimum distance between points in the tip region. The linear extrapolation gives $t_{pinch} \simeq 7.6 r_b^3(0)$

towards a close to linear behavior as the resolution is increased. Extrapolation towards $z_{min} = 0$ thus gives a reliable estimate of the time required for reconnection. Although the walls of the gap do not interact physically, errors of our boundary integral description grow large as two surfaces become close to each other. The reason is that the distance λ between points varies on scale z_{min} close to the minimum, so the grid spacing δ always needs to be smaller than z_{min} .

From the simulations we deduce the values $r_0 = 10$ and $\tau_0 = 7.6$ for the reduced retraction length and time already reported in section 2. Here the underlying assumption is that the dynamics is controlled by the local gap width alone. To test this idea, we have computed a sequence of pinch events as shown in figure 4. When z_{min} has gone down to about 10 % of the local gap radius $w/2$, the gap is cut at about $w/2$ behind the minimum and new points are introduced along the new surface. Our method of redistributing points

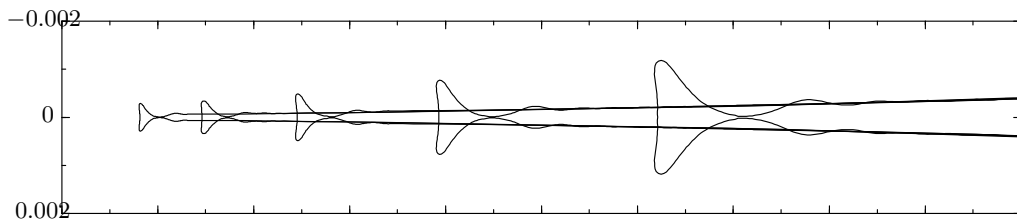


FIGURE 4. Successive entrainment of voids during the coalescence for an initial liquid bridge radius of $r_b = 0.008$. After every reconnection, the void is extracted from the profile and a new computation begins, with a null initial velocity field.

automatically introduced a certain smoothing, which was enough for the simulation to continue. Obtaining a new initial condition for the velocity profile proved to be much more difficult. Simply extrapolating the velocity potential φ before the surgery to the new initial condition led to instabilities that could no longer be controlled numerically, so instead we had to put the velocity field to zero. This is justified by the fact that the gap position very quickly re-assumes its retraction velocity after the bubble is left behind, as we discuss in more detail below.

As illustrated in figure 4, this leads to a self-similar succession of pinch-off events. Each simulation was started from a new value of the bridge radius r_b^n . The typical gap width at the meniscus is then $w = (r_b^n)^2$. A more quantitative test of the scalings employed in section 2 is presented in figure 5, where we plot the bridge radius r_b as a function of time and, in the inset, $r_c/\tau_c = (r_0/\tau_0)/r_b^n$ as function of the bridge radius at the time of pinching. The excellent agreement with the predicted scaling behavior confirms our assumption that the local dynamics only depends on the gap width at the corresponding radius r_b^n .

We also did not follow the evolution of the bubble after it was cut off from the gap. Since it starts from a highly non-circular shape, it is expected to perform large amplitude oscillations. Remembering that the bubble is really a torus in three-dimensional space, it will also be unstable with respect to the Rayleigh instability (Drazin & Reid 1982)

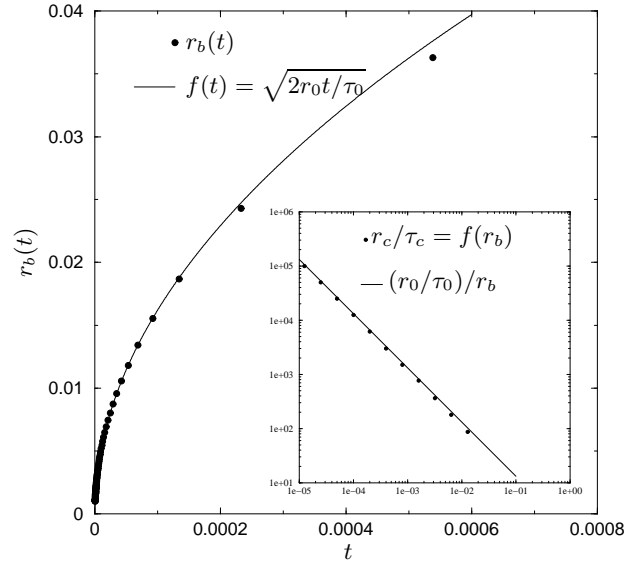


FIGURE 5. The minimum radius r_b as a function of time (dots), compared to the theoretical prediction $\sqrt{2r_0 t / \tau_0}$ (full line). Inset: the ratio r_c / τ_c as a function of the initial radius r_b^2 varying between $1.25 \cdot 10^{-5}$ and $1.28 \cdot 10^{-2}$. The time for pinching τ_c was approximated using a linear extrapolation of z_{min} . The numerical results show very good agreement with the expected scaling law.

and break up into a sequence of smaller bubbles. Evidently, this instability breaks the rotational symmetry and is thus well beyond the scope of the present work.

5. Dynamics of retraction

We now study the individual retraction events, characterized by a mass of fluid being accelerated by two line forces, in greater detail. Thus if

$$\frac{dr_b}{dt} = v_{tip}$$

is the velocity of the receding tip, the force balance reads

$$\frac{d}{dt} \left(M_{tip} \frac{dr_b}{dt} \right) = 2, \quad (5.1)$$

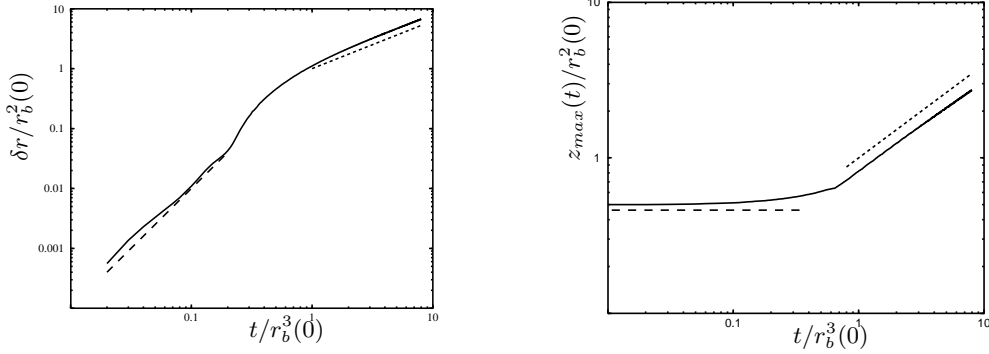


FIGURE 6. Two quantities characterizing retraction, $\delta r = r_b(t) - r_b(0)$ and z_{max} as functions of time in rescaled units. Long-dashed and dotted lines represent power-law approximations to the early and long-time behavior, respectively. We find $\delta r \propto t^2$ for early times, while z_{max} remains constant. For late times $\delta r \propto t^{0.8}$ and $z_{max} \propto t^{0.6}$; both behaviors are in agreement with (5.2).

where M_{tip} is the mass being accelerated. This “added mass” is being pushed along by the structure of maximum radius z_{max} that is forming at the end of the gap, and thus $M_{tip} \approx Cz_{max}^2$ (Landau & Lifschitz 1982), where C is a numerical constant coming from the geometry of the void profile. Hence the equation of motion becomes

$$\frac{d}{dt} \left(Cz_{max}^2 \frac{dr_b}{dt} \right) = 2. \quad (5.2)$$

For short times, the bubble does not have time to grow, so z_{max} is approximately constant and given by the initial gap radius: $z_{max} \approx r_b^2(0)/2$. This corresponds to a constant mass being accelerated by a constant force, and (5.2) leads to a quadratic growth of the retraction distance $\delta r_b(t) = r_b(t) - r_b(0) \propto t^2$. This is confirmed by the early time behavior of $\delta r_b(t)$ as shown in figure 6. Note that, consistent with (5.2), z_{max} remains constant.

After this initial period of acceleration, the bubble radius z_{max} starts to grow and the speed of retraction v_{tip} reaches a maximum, as seen in figure 7. This maximum must be set by the initial width w of the gap, and thus dimensional arguments lead to

$$v_c \approx \sqrt{2/w}. \quad (5.3)$$

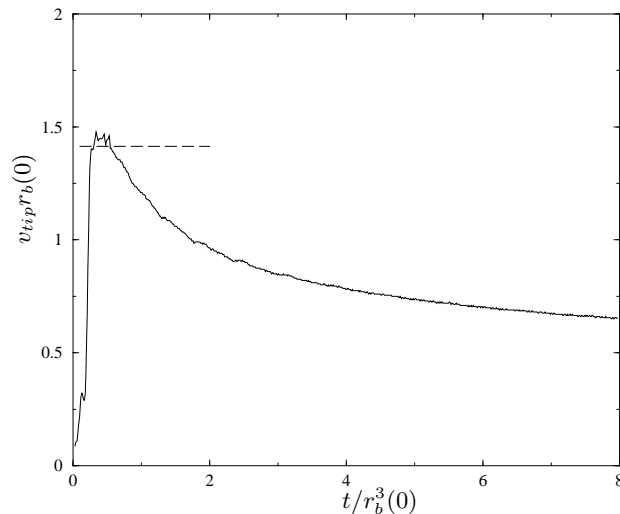


FIGURE 7. The speed of the retracting bridge $v_{tip} = dr_b(t)/dt$ as a function of time in rescaled units. The Culick-Taylor velocity ($\sqrt{2}$ in these units) is represented by the dashed segment.

The prefactor in (5.3) comes from balancing the inertial term $v_c^2/2$ with the surface tension force κ in (2.2), in analogy with the arguments of Culick and Taylor (Culick 1960; Taylor 1959) for receding soap films. The curvature κ has been approximated by $1/w$. As confirmed by figure 7, the maximum of v_{tip} is well approximated by the estimate (5.3).

After reaching a maximum, the speed of retraction decreases steadily, as the bubble grows and with it the added mass that has to be dragged along. The transversal bubble expansion is due to the rapid fluid motion along its sides which, according to Bernoulli's equation (2.2), causes an under-pressure. Conversely, at the stagnation point behind the bubble the pressure is high and the bubble is curved inward (cf. figure 2). We do not yet have a fully quantitative theory of the bubble expansion, since this would require a precise knowledge of the bubble's shape. Namely, the fluid speed v_m past the crest of the bubble is determined by its curvature κ_c (Lamb 1993): $v_m = v_{tip}\kappa_c z_{max}$, in analogy to the flow past an ellipsoidal body. To close the system of equations, we would need an expression

for κ_c . However, we notice from figure 6 that the temporal growth of the bubble size z_{max} is well described by a power law: $z_{max} \propto t^{0.6}$. Plugging this into equation (5.2) we find

$$\delta r_b \propto t^{0.8}, \quad (5.4)$$

in good agreement with simulations, cf. figure 6. The range of validity of the power laws proposed here can of course never exceed an order of magnitude, since the gap pinches off after time $t \approx 10r_b^3$.

Eventually, when the toroidal bubble separates from the gap, the velocity v_{tip} has decreased to about half of v_c . Therefore, the effect of the dynamical pressure $v_{tip}^2/2$ is reduced considerably relative to the capillary pressure. Numerically, we find that the capillary force is at least 4 times bigger than the dynamical pressure, which indicates that the velocity field can safely be neglected at reconnection, as we are forced to do owing to limitations of our numerical technique.

6. Discussion

We have shown that the merging of low viscosity fluid droplets leads to a self-similar sequence of void entrapments. It is interesting to note that the same power law behavior (2.6) of r_b can be formally derived from a continuous evolution if v_{tip} is assumed to be the Culick velocity (5.3). If the gap width w is estimated from the geometrical constraint $w \approx r_b^2$, this immediately leads to $\partial_t r_b \approx \sqrt{2}/r_b$, which can be integrated to give a power $t^{1/2}$. This is the argument given in (Eggers *et al.* 1999), which did not take reconnection into account. The reason it ends up to give the correct answer (apart from the prefactor) is that the size of the gap tip is rescaled to agree with the geometrical estimate (2.3) at each reconnection event. Thus although the bubble actually grows to a much larger size than r_b^2 , the balance implied by the above argument is actually true *on average*.

It might be equally tempting (Lister 2002) to apply the same reasoning to the force balance (5.1), by approximating (at least on average) the added mass by $M_{tip} \approx Cz_{max}^2 \propto r_b^4$. Integrating the corresponding equation of motion leads to $r_b \propto t^{2/5}$. This apparent paradox is explained by the fact that the reconnection events destroy the momentum conservation implied by (5.1). Owing to bubble growth, momentum is distributed over a much larger volume than estimated from the simple geometrical argument. Accordingly, in the asymptotic limit of $t \ll 1$ one obtains a motion that is *faster* than that given by the full calculation including reconnection.

We would finally like to point out some questions inspired by this work. Firstly, it would be nice to develop a more complete theory of the bubble growth at the end of the receding meniscus. Secondly, we are not yet able to fully treat the velocity field after reconnection. Such a treatment may lead to an increase in fluctuations and perhaps some randomness during retraction. As pointed out in (Oguz & Prosperetti 1990), a finite velocity of approach will increase the likelihood of bubble entrapment during coalescence. Other interesting generalizations not yet considered in the present paper are the effect of an external fluid as well as viscous corrections. Clearly, a number of theoretical questions remain open. Perhaps more importantly, detailed experimental studies are called for, for example to verify the phenomenon of bubble entrainment predicted by our analysis.

It is our pleasure to thank Stéphane Zaleski for its constant encouragement during this work.

REFERENCES

- AMAROUCHENE, A., CRISTOBAL, G. & KELLAY, H. 2001 Noncoalescing drops. *Phys. Rev. Letters* **87**, 206104–1–206104–4.

- BAKER, G. R., MEIRON, D. I. & ORSZAG, S. A. 1980 Vortex simulations of the rayleigh-taylor instability. *Phys. Fluids* **23**, 1485–1490.
- BRADLEY, S. G. & STOW, C. D. 1978 Collisions between liquid drops. *Phil. Trans. R. Soc. London A* **287**, 635–675.
- CHAUDHARY, K. C. & MAXWORTHY, T. 1980 The nonlinear capillary instability of a liquid jet. part3. experiments on satellite drop formation and control. *J. Fluid Mech.* **96**, 287–297.
- CROWDY, D. 2002 Exact solutions for the viscous sintering of multiply-connected fluid domains. *J. Eng. Math.* **42**, 225–242.
- CROWDY, D. To appear Viscous sintering of unimodal and bimodal cylindrical packings with shrinking pores. *Eur. J. Appl. Math.*
- CULICK, F. E. C. 1960 Comments on a ruptured soap film. *J. Appl. Phys.* **31**, 1128.
- DRAZIN, P. G. & REID, W. H. 1982 *Hydrodynamic stability*. Cambridge Univ. Pr.
- EGGERS, J. 1997 Nonlinear dynamics and breakup of free surface flows. *Rev. Mod. Phys.* **69**, 865–929.
- EGGERS, J. 1998 Coalescence of spheres by surface diffusion. *Phys. Rev. Letters* **80**, 2634–2637.
- EGGERS, J., LISTER, J. R. & STONE, H. A. 1999 Coalescence of liquid drops. *J. Fluid Mech.* **401**, 293–310.
- FRENKEL, J. 1945 Viscous flow of crystalline bodies under the action of surface tension. *J. Phys. (Moscow)* **9**, 385–391.
- HOPPER, R. W. 1990 Plane stokes flow driven by capillarity on a free surface. *J. Fluid Mech.* **213**, 349–375.
- HOPPER, R. W. 1993 Coalescence of two viscous cylinders by capillarity: Part i. theory. *J. Am. Ceram. Soc.* **76**, 2947–2952.
- JURY, S. I., BLADON, P., KRISHNA, S. & CATES, M. E. 1999 Tests of dynamical scaling in three-dimensional spinodal decomposition. *Phys. Rev. E* **59**, R2535–R2538.
- LAFAURIE, B., NARDONE, C., SCARDOVELLI, R., ZALESKI, S. & ZANETTI, G. 1994 Modelling merging and fragmentation in multiphase flows with surfer. *J. Comp. Phys.* **113**, 134–147.
- LAMB, H. 1993 *Hydrodynamics*. Cambridge.
- LANDAU, L. D. & LIFSHITZ, E. M. 1982 *Fluid Mechanics*. Oxford.

- LISTER, J. R. 2002 This argument was quoted to us by J. R. Lister .
- MACPHEE, A. G., TATE, M. W., POWELL, F., YUE, Y., RENZI, M. J., ERCAN, A., NARAYANAN, S., FONTES, E., WALTHER, J., SCHALLER, J., GRUNER, S. M. & WANG, J. 2002 X-ray imaging of shock waves generated by high-pressure fuel sprays. *Science* **295**, 1261–1263.
- MARTINEZ-HERRERA, J. I. & DERBY, J. J. 1995 Viscous sintering of spherical particles via finite element analysis. *J. Am. Ceram. Soc.* **78**, 645–649.
- MENCHACA-ROCHA, A., MARTNEZ-DVALOS, A., NEZ, R., POPINET, S. & ZALESKI, S. 2001 Coalescence of liquid drops by surface tension. *Phys. Rev. E* **63**, 046309–1–046309–5.
- NIKOLAYEV, V. S., BEYSENS, D. & GUENOUN, P. 1996 New hydrodynamic mechanism for drop coarsening. *Phys. Rev. Letters* **76**, 3144–3147.
- OGUZ, H. N. & PROSPERETTI, A. 1989 Surface-tension effects in the contact of liquid surfaces. *J. Fluid Mech.* **203**, 149–171.
- OGUZ, H. N. & PROSPERETTI, A. 1990 Bubble entrainment by the impact of drops on liquid surfaces. *J. Fluid Mech.* **219**, 143–179.
- PRESS, W. H., TEUKOLSKY, S. A., VETTERLING, W. T. & FLANNERY, B. P. 1992 *Numerical Recipes*. Cambridge University Press.
- RICHARDSON, S. 1992 Two-dimensional slow viscous flows with time-dependent free boundaries driven by surface tension. *Euro. J. Appl. Math* **3**, 193–207.
- TAYLOR, G. I. 1959 The dynamics of thin sheets of fluid. iii. disintegration of fluid sheets. *Proc. R. Soc. Lond.* **A253**, 313–321.
- VERDIER, C. 2000 Coalescence of polymer droplets: experiments on collision. *C.R. Acad. Sci. Paris Ser. IV* **1**, 119–126.
- WALLACE, D. B. 2001 Ink-jet applications, physics, and modelling - an industrial/applied research view. In *talk delivered at IMA "Hot Topics" Workshop: Analysis and Modeling of Industrial Jetting Processes*, <http://www.ima.umn.edu/multimedia/abstract/1-10abs.html#wallace>.
- YIANTSOS, S. G. & DAVIS, R. H. 1991 Close approach and deformation of two viscous drops due to gravity and van der waals forces. *J. Coll. & Int. Sci.* **144**, 412–433.